ELSEVIER

Materials Characterization 45 (2000) 143–152

MATERIALS
CHARACTERIZATION

Martensitic transformation of quaternary $Ti_{50.5-X}Ni_{49.5}Zr_{X/2}Hf_{X/2}$ (X = 0–20 at.%) shape memory alloys

S.F. Hsieh[a], S.K. Wu[b,*]

[a]Department of Mold and Die Engineering, National Kaohsiung Institute of Science and Technology, Kaohsiung 800, Taiwan
[b]Institute of Materials Science and Engineering, National Taiwan University, Taipei 106, Taiwan

Received 9 February 2000; accepted 10 March 2000

Abstract

Martensitic transformation of $Ti_{50.5-X}Ni_{49.5}Zr_{X/2}Hf_{X/2}$ quaternary alloys (X = 0–20 at.%) is studied by different thermo-mechanical treatments. These alloys have one-stage B2↔B19′ transformation and exhibit $\geq$ 80% shape memory recovery. Their DSC forward transformation peak M^* can be raised from 50°C to 323°C with transformation hysteresis being slightly larger than that of $Ti_{50.5-X}Ni_{49.5}Zr_X$ alloys. In the early 10 cycles, thermal cycling can depress the M^* temperature more significantly in $Ti_{35.5}Ni_{49.5}Zr_{7.5}Hf_{7.5}$ than in $Ti_{35.5}Ni_{49.5}Zr_{15}$ due to the former alloy having higher hardness in the matrix. Martensite stabilization can be induced by cold rolling at room temperature. The strengthening effects of cold rolling and thermal cycling on Ms temperature are found to follow Ms = $T_o - K\Delta\sigma_y$, in which K values are related to the as-annealed hardness of these alloys. $Ti_{30.5}Ni_{49.5}Zr_{10}Hf_{10}$ alloy, aged in martensite phase can cause the phenomenon of thermal-induced martensite stabilization. © 2000 Elsevier Science Inc. All rights reserved.

Keywords: Martensitic transformation; Quaternary alloys; Shape memory recovery

1. Introduction

Among many shape memory alloys (SMAs), TiNi-based alloys are the most popular due to their superior properties in the shape memory effect (SME) and pseudoelasticity (PE) [1,2]. However, the addition of a third element has a substantial effect on phase transformation behaviors in TiNi alloys. The Ms temperature decreases monotonically following substitution for Ni with Fe, Al, and Co elements [3–5] but increases remarkably following substitution of Ni with Au, Pd, and Pt in amounts not less than 15 to 20 at.% [6–8], in which they are called "high-temperature SMAs". However, the high cost of precious metals limits the practical applications of these high-temperature SMAs. For this reason, other low-cost TiNiX SMAs need to be investigated. Among them, the most significant candidates are TiNiZr and TiNiHf alloys with Zr and Hf being used to replace Ti in these SMAs.

Three phases (Ti,Zr)Ni, $(Ti,Zr)_2Ni$ and the λ_1 phase are observed in Ti-rich $Ti_{53-X}Ni_{47}Zr_X$ alloys with the Zr content in the range 5–20 at.% at room temperature. Here, the λ_1 phase is a TiNiZr ternary solid solution and the (Ti,Zr)Ni phase can exhibit the

---

* Corresponding author. Tel.: +886-2-2363-7846; fax: +886-2-2363-4562.
E-mail address: skw@ccms.ntu.edu.tw (S.K. Wu).

PII: S1044-5803(00)00068-1

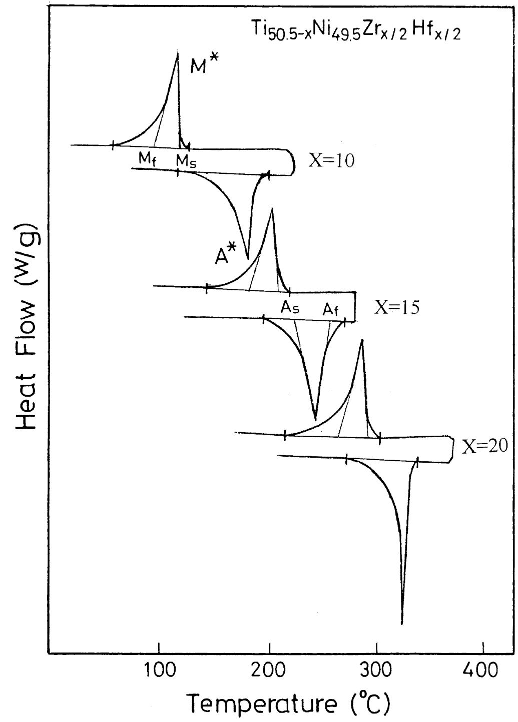

Fig. 1. DSC curves of as-annealed $Ti_{50.5-X}Ni_{49.5}Zr_{X/2}Hf_{X/2}$ alloys ($X = 0-20$ at.%). M^* and A^* are peak temperatures of forward and reverse martensitic transformation, respectively.

B2↔B19′ one-stage martensitic transformation with Ms temperature higher than 100°C [9]. Meisner and Sivokha [10] reported that $(Ti,Zr)_2Ni_7$, $(Ti,Zr)_7Ni_{10}$, and NiZr phases can be observed in the Ni-rich $Ti_{50-X}Ni_{50}Zr_X$ alloys with Zr content in the range 30–50 at.% at room temperature. The lattice parameters of $Ti_{50.5-X}Ni_{49.5}Zr_X$ alloys could be changed by Zr content in the range 5–20 at.% [11]. Mulder et al. [12] reported that the decrease of transformation temperature in thermally-cycled $Ti_{31.5}Ni_{48.5}Zr_{20}$ alloy is affected by the precipitates.

The transformation behavior and shape memory characteristics of Ti-rich TiNiZr alloys have been reported under various thermo-mechanical treatments, such as thermal cycling, aging, and cold rolling [13]. However, $Ti_{50.5-X}Ni_{49.5}Zr_X$ alloys with Ti being partially replaced by Hf, are seldom reported to have their transformation behavior and shape memory characteristics affected by these treatments. The aim of the present work is to investigate systematically the general characteristics of Ti-rich TiNiZrHf quaternary SMAs. The transformation behavior and shape recovery of these alloys will be compared with those of Ti-rich TiNiZr ternary ones. The effects of aging, cold rolling, and thermal cycling on these alloys will also be discussed in this study.

2. Experimental procedure

A conventional tungsten arc melting technique was employed to prepare $Ti_{50.5-X}Ni_{49.5}Zr_{X/2}Hf_{X/2}$ (A alloys) alloys with $X = 0-20$ at.%. These alloys' compositions are based on $Ti_{50.5-X}Ni_{49.5}Zr_X$ alloys (B alloys) which have been intensively studied in our previous work [13]. Titanium (purity 99.7 wt.%), nickel (purity 99.9 wt.%), zirconium (purity 99.8 wt.%) and hafnium (purity, 99.2 wt.%), totaling about 100 g, were melted and remelted at least six times in an argon atmosphere. A pure titanium button was also melted and used as a getter. The mass loss during melting was negligibly small. The as-melted buttons were homogenized at 950°C for 72 h and then

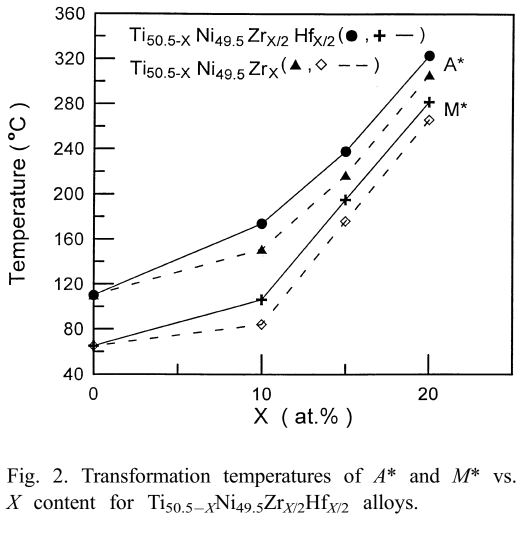

Fig. 2. Transformation temperatures of A^* and M^* vs. X content for $Ti_{50.5-X}Ni_{49.5}Zr_{X/2}Hf_{X/2}$ alloys.

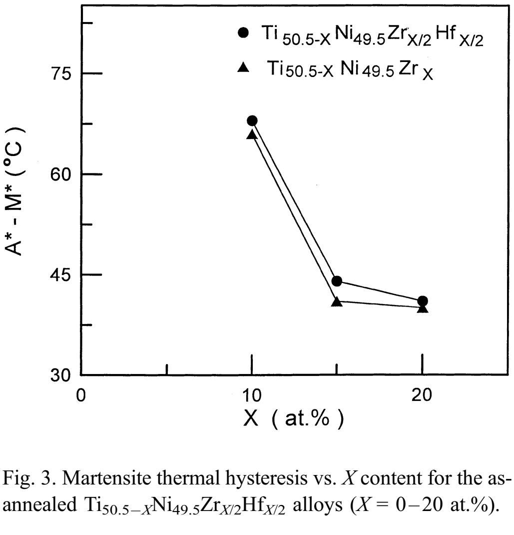

Fig. 3. Martensite thermal hysteresis vs. X content for the as-annealed $Ti_{50.5-X}Ni_{49.5}Zr_{X/2}Hf_{X/2}$ alloys ($X = 0-20$ at.%).

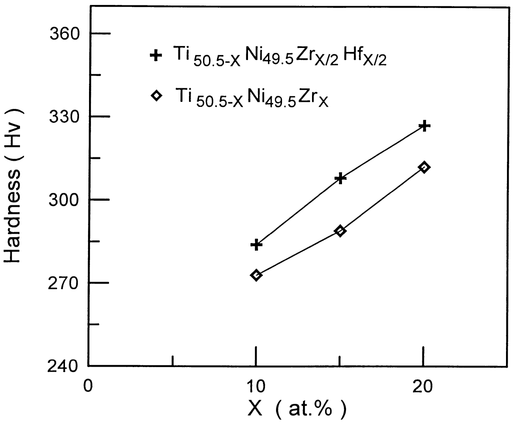

Fig. 4. Hardness vs. X content for the as-annealed $Ti_{50.5-X}Ni_{49.5}Zr_{X/2}Hf_{X/2}$ and $Ti_{50.5-X}Ni_{49.5}Zr_X$ alloys (X = 0–20 at.%).

quenched in water. The homogenized buttons were cut into several plates with a low speed diamond saw, and then annealed at 900°C for 2 h and quenched in water. After the annealing treatment, three experimental procedures were conducted. First, some plates were sealed in evacuated quartz tubes, aged at 285°C for 2 days to 50 days and then quenched in water. Second, some plates were cold-rolled at room temperature to 5%, 10%, 15% and 25% reduction in their thicknesses. Third, other plates were subjected to thermal cycling N times from 0°C to 300°C with N = 1–100 cycles. Specimens for DSC measurements, hardness tests, shape recovery tests and microstructural observations were carefully cut from plates treated by the above three procedures. DSC measurements were made with a Dupont 9990 thermal analyzer equipped with a quantitative scanning system 910 DSC cell for controlled heating and cooling runs on samples encapsulated in an aluminum pan.

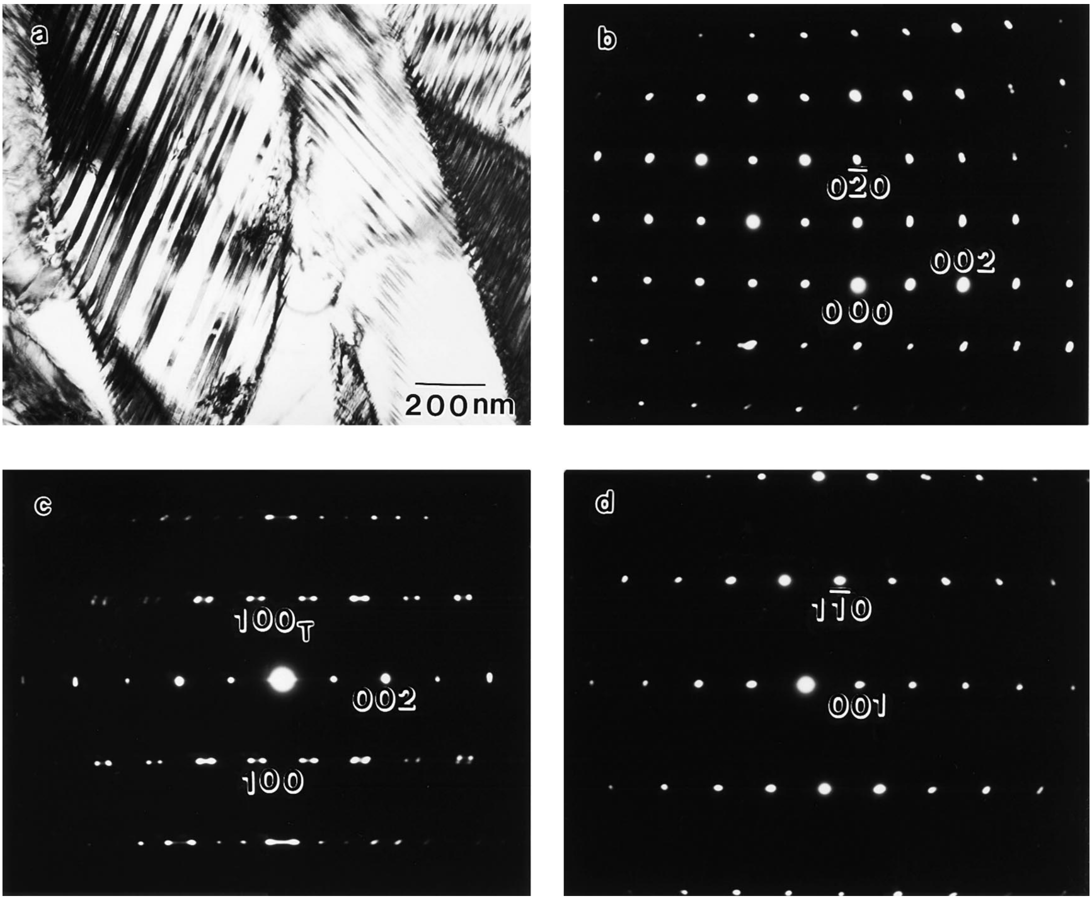

Fig. 5. (a) TEM bright-field image of as-annealed $Ti_{30.5}Ni_{49.5}Zr_{10}Hf_{10}$ alloy. (b)–(d) Selected area diffraction patterns (SADPs) of (a) with (b) $[100]_M$ zone axis, (c) $[010]_M$ zone axis and (d) $[110]_M$ zone axis.

The running temperature range was from 0°C to 400°C with a heating and cooling rate of 10°C/min. Specimens for the hardness test were first mechanically polished and then subjected to measurement in a microVickers hardness tester with a 500 g load at room temperature. For each specimen, the average hardness value was taken from at least five test readings. The microstructural observations were made by transmission electron microscopy (TEM) with a JOEL-100CXII microscope equipped with a conventional double-tilting stage. The shape recovery measurement was performed as described in an earlier report [14]. The chemical composition analysis for each phase was performed using a JOEL JXA-8600SX electron probe microanalyzer (EPMA) equipped with a WDX analysis system.

3. Experimental results and discussion

3.1. Transformation behavior in $\mathrm{Ti}_{50.5-X}\mathrm{Ni}_{49.5}\mathrm{Zr}_{X/2}\mathrm{Hf}_{X/2}$ *alloys*

Fig. 1 shows the experimental results of DSC measurements for homogenized $\mathrm{Ti}_{50.5-X}\mathrm{Ni}_{49.5}\mathrm{Zr}_{X/2}\mathrm{Hf}_{X/2}$ alloys with $X = 0-20$ at.% in both forward and reverse transformations, respectively. The peaks M^* and A^* (including Ms, Mf, As and Af points) shown in Fig. 1 are associated with the one-stage martensite transformation of B2↔B19′. The transformation peaks M^* and A^* vs. X of Fig. 1 are plotted in Fig. 2. From Fig. 2, the M^* temperature increases from 50°C to 323°C with increasing X content. Therefore, based on the results of Fig. 2, a quaternary TiNiZrHf SMA with a desired transformation temperature can be obtained by carefully controlling its corresponding X content. For the same X, transformation peak temperatures of A alloys are higher than those of B alloys. Based on the report of Han et al. [15], phase transformation temperatures of $\mathrm{Ti}_{36.5}\mathrm{Ni}_{48.5}\mathrm{Hf}_{15}$ alloy increase largely by using Hf to substitute Ti. These temperatures are also higher than those of $\mathrm{Ti}_{36.5}\mathrm{Ni}_{48.5}\mathrm{Zr}_{15}$ alloy. Similar characteristic can be seen in Fig. 2 in which A alloys have Ti being substituted partially by Hf but B alloys do not.

Transformation thermal hysteresis (A^*-M^*) of A and B alloys decreases with increasing X content, as shown in Fig. 3. It is reported that the value of (A^*-M^*) essentially depends on the degree of structural change between parent and martensite in NiTi-based alloys [16,17]. The $\mathrm{Ti}_{50}\mathrm{Ni}_{50}$ SMA, NITINOL, has a transformation hysteresis of about 30 K and a monoclinic martensite structure. The hysteresis reduction is realized in $\mathrm{Ti}_{50}\mathrm{Ni}_{50-X}\mathrm{Cu}_X$ SMAs, in which the copper addition changes the martensite structure to an orthorhombic one and reduces the hysteresis to 10–15 K. Subsequently, the R-phase transformation is identified in the binary TiNi alloys under the combination of cold working and heat treatment and its hysteresis is further reduced to 2 K. By contrast, a wide hysteresis up to 100 K is also achieved by a

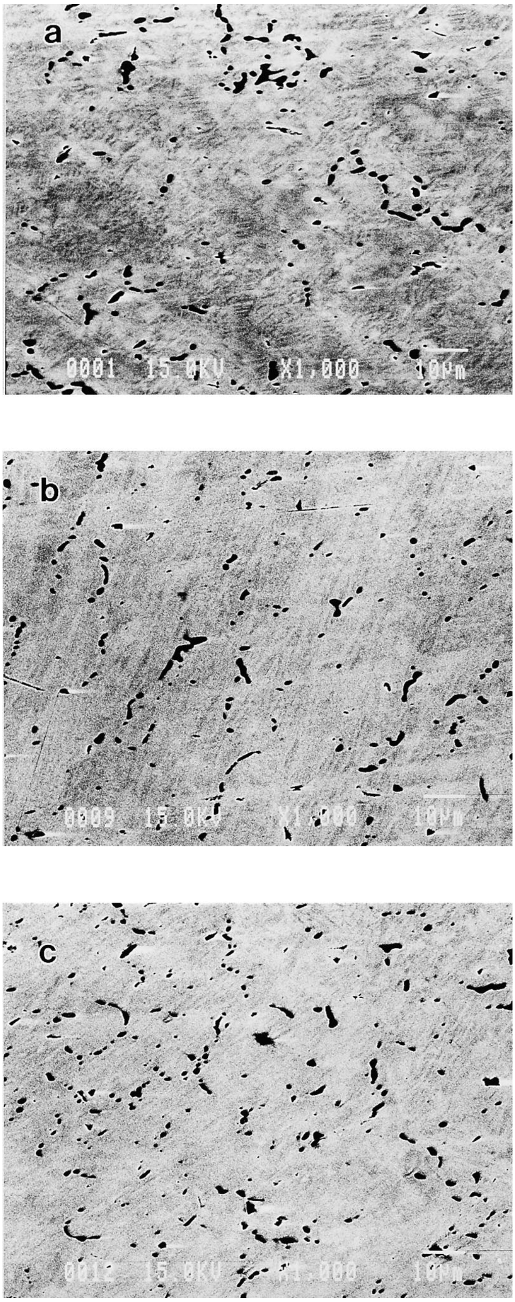

Fig. 6. Backscattering electron images (BEIs) of as-annealed $\mathrm{Ti}_{50.5-X}\mathrm{Ni}_{49.5}\mathrm{Zr}_{X/2}\mathrm{Hf}_{X/2}$ alloys with (a) $X = 10$, (b) $X = 15$, (c) $X = 20$ at.%.

Table 1
Chemical composition of matrix and second phase particles of as-quenched $Ti_{50.5-X}Ni_{49.5}Z_{X/2}Hf_{X/2}$ alloys with $X = 10$, 15, and 20 at.% detected by EPMA

950°C × 24 h as-quenched

Phases		Composition (at.%) Ti	Ni	Zr	Hf	(Ti + Zr + Hf)/ Ni ratio
$X = 10$	M	41.47	48.92	4.68	4.93	1.04
	S	53.04	36.97	6.18	3.81	1.7
$X = 15$	M	36.60	49.09	6.76	7.55	1.03
	S	48.27	37.23	7.36	7.14	1.69
$X = 20$	M	31.24	49.42	9.36	9.98	1.02
	S	44.02	37.94	10.32	7.72	1.64

Note. M: matrix; S: second phase particles.

combination of a dispersion of fine niobium particles and cold working. From Fig. 3, the hysteresis effect of A alloys is larger than that of B alloys. We propose that the added Hf in Ti-rich TiNiZrHf alloys may not only increase the transformation hysteresis, but also strengthen the matrix due to solid solution hardening, as shown in Fig. 4.

Fig. 5a shows the TEM bright-field image of martensite in annealed $Ti_{30.5}Ni_{49.5}Zr_{10}Hf_{10}$ alloy. Fig. 5b–d shows the SADPs of Fig. 5a with $[100]_M$, $[010]_M$ and $[110]_M$ zones, respectively. Han et al. [15] found that $Ti_{36.5}Ni_{48.5}Hf_{15}$ alloy is a monoclinic B19′ structure with $a = 0.293$ nm, $b = 0.411$ nm, $c = 0.473$ nm and $\beta = 100.4°$. The SADPs of Fig. 5 coincide with the results of Han et al. [15]. Therefore, the structure of martensite in $Ti_{30.5}Ni_{49.5}Zr_{10}Hf_{10}$ alloy is still monoclinic. From Figs. 1 and 5, one can find that the transformation sequence of martensite in Ti-rich TiNiZrHf alloys is the B2↔B19′ one-stage transformation.

Fig. 6a–c shows the EPMA BEIs of 900°C annealed $Ti_{50.5-X}Ni_{49.5}Zr_{X/2}Hf_{X/2}$ alloys with $X = 10$, 15, 20 at.%, respectively. The intensity of the backscattered electron image is proportional to the atomic number of the individual element in the illuminated area. A great number of second phase particles are found around the grain boundaries of the matrix. The chemical compositions of the matrix and second phase particles by EPMA analysis are shown in Table 1. The ratio (Ti + Zr + Hf)/Ni of the matrix and that of the second phase particles are also shown in Table 1. According to our previous work [9], the results of Table 1 indicate that the matrix in Fig. 6 is the (Ti,Zr,Hf)Ni phase (Zr and Hf atoms are dissolved in the TiNi phase) and the black particles are the λ_1 phase. The volume fraction of second phase particles occupies about 4% for these alloys.

Fig. 7 shows the shape recovery of A and B alloys. Despite the existence of many second phase particles, these alloys still exhibit good shape recovery up to about 80%. The shape recovery of A alloys is slightly more than that of B alloys after the specimens were heated to 450°C. This feature is closely related to Hf in solid-solution in the matrix of Ti-rich TiNiZrHf alloys. It has been reported that the shape recovery of TiNi alloys can be increased by different strengthening/hardening processes [18]. Second phase particles do not transform martensitically when the temperature changes. They are characterized by high brittleness and limited plasticity. However, in the matrix, the hardening effect of A alloys is slightly larger than that of B alloys due to Hf solid solution hardening, as shown in Fig. 4. Therefore, the shape recovery

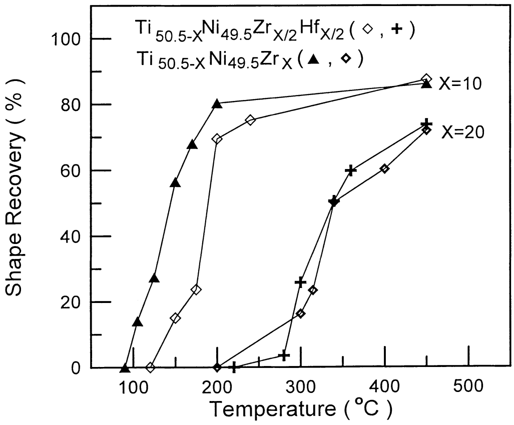

Fig. 7. Shape recovery vs. heating temperature for the as-annealed $Ti_{50.5-X}Ni_{49.5}Zr_{X/2}Hf_{X/2}$ and $Ti_{50.5-X}Ni_{49.5}Zr_{X}$ alloys.

Table 2
DSC peak temperature A_1*, M_1*, A_2* and the hardness of $Ti_{35.5}Ni_{49.5}Zr_{7.5}Hf_{7.5}$ alloy under various thickness reductions of cold rolling at room temperature

Thickness of cold rolling reduction (%)	A_1* (°C)	ΔH_{h1} (J/g)	M_1* (°C)	ΔH_C (J/g)	A_2* (°C)	ΔH_{h2} (J/g)	Hardness (Hv)
0	238	26.81	195	24.10	226	23.48	308
5	301	19.33	160	18.32	220	14.50	368
10	341	7.47	132	7.27	190	5.64	407
15	413	6.37	103	6.08	165	5.12	432
25	510	4.12	50	3.91	126	3.53	496

of A alloys is also slightly more than that of B alloys, as demonstrated in Fig. 7.

3.2. Cold rolling effect on the $Ti_{35.5}Ni_{49.5}Zr_{7.5}Hf_{7.5}$ alloy

The effects of cold rolling on martensitic transformation of $Ti_{36.5}Ni_{48.5}Zr_{15}$ and $Ti_{35.5}Ni_{49.5}Zr_{15}$ alloys have been systematically studied previously [13]. The phenomenon of martensite stabilization is observed in the cold-rolled Ti-rich TiNiZr martensite. In the present study, the $Ti_{35.5}Ni_{49.5}Zr_{7.5}Hf_{7.5}$ alloy is plastically deformed by cold rolling at room temperature.

Table 2 shows the detailed results of DSC and hardness measurements for various amounts of cold rolling in the $Ti_{35.5}Ni_{49.5}Zr_{7.5}Hf_{7.5}$ alloy in which the reverse transformation peaks A_1* and A_2*, respectively indicate the first and second heating cycle for the specimen just after the cold rolling. In Table 2, A_1* temperatures significantly increase, but A_2* decrease, along with increased cold rolling. Besides, the M* temperature is also found to decrease with increased cold rolling. The above phenomenon is regarded as the mechanically-induced martensite stabilization in $Ti_{35.5}Ni_{49.5}Zr_{7.5}$ $Hf_{7.5}$ alloy. The same behavior is also reported in $Ti_{50}Ni_{50}$, $Ti_{51}Ni_{49}$, and $Ti_{35.5}Ni_{49.5}Zr_{15}$ alloys [13,19]. After the occurrence of the first reverse transformation of $B19' \rightarrow B2$, the martensite stabilization dies out and A_2* temperatures are lower than A_1*. In Fig. 8a, ΔA* (the difference between A_1* and A_2*) stands for the degree of martensite stabilization. From Fig. 8a, the ΔA* of $Ti_{35.5}Ni_{49.5}Zr_{7.5}$ $Hf_{7.5}$ alloy (ΔA* = 384°C) is larger than that of $Ti_{35.5}Ni_{49.5}Zr_{15}$ alloy (ΔA* = 351°C) [13] for the same 25% cold-rolled specimen. Fig. 8b shows that the increment of hardness under the same cold rolling, is about 188 Hv for $Ti_{35.5}Ni_{49.5}Zr_{7.5}Hf_{7.5}$ alloy and about 176 Hv for $Ti_{35.5}Ni_{49.5}Zr_{15}$ alloy [13]. The as-annealed hardness of the former alloy is slightly greater than that of the latter due to Hf dissolved in the matrix. We suggest that the dislocation movement may be hindered more in the $Ti_{35.5}Ni_{49.5}Zr_{7.5}Hf_{7.5}$ alloy than in the $Ti_{35.5}Ni_{49.5}$ Zr_{15} alloy and cause the harder $Ti_{35.5}$-$Ni_{49.5}Zr_{7.5}$ $Hf_{7.5}$ alloy to have a higher martensite stabilization under the same level of cold rolling, as demonstrated in Fig. 8.

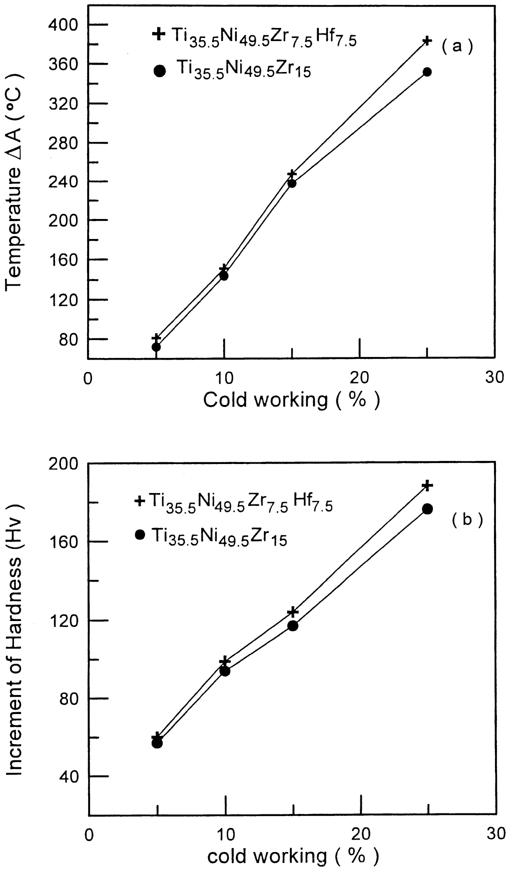

Fig. 8. (a) The degree of martensite stabilization (ΔA*) and (b) the increment of hardness (ΔHv) vs. degree of cold rolling for the $Ti_{35.5}Ni_{49.5}Zr_{7.5}Hf_{7.5}$ alloy.

3.3. Thermal cycling effects on the $Ti_{35.5}Ni_{49.5}Zr_{7.5}Hf_{7.5}$ alloy

Fig. 9a and b shows peak temperatures *M**, *A** and hardness Hv, respectively, vs. thermal cycles *N* for annealed $Ti_{35.5}Ni_{49.5}Zr_{15}$ and $Ti_{35.5}Ni_{49.5}Zr_{7.5}Hf_{7.5}$ alloys. *M** and *A** temperatures decrease, but the hardness Hv increases with increasing thermal cycling. It has been proposed that this feature comes from the influence of dislocations induced by thermal cycling [20]. *A** and *M** decrease quickly for the first 10 cycles, with the decrement being about 28°C for Fig. 9b and about 25°C for Fig. 9a. The increase in hardness shown in Fig. 9b ($\Delta Hv = 48$) is greater than that of Fig. 9a ($\Delta Hv = 43$) after $N = 10$ cycles. This indicates that the $Ti_{35.5}Ni_{49.5}Zr_{7.5}Hf_{7.5}$ alloy can induce more dislocations than the $Ti_{35.5}Ni_{49.5}Zr_{15}$ alloy in the early thermal cycling. We suggest that the volume change during the martensitic transformation can produce a complex stress field at the interfaces of second phase particles and B2/B19′ matrix during thermal cycling. This complex stress field can enhance the dislocation multiplication, which increases the hardness of the alloy and depresses its *M** temperature. In Fig. 9, after 75 cycles, the *M** and *A** temperatures reach a constant value. This may indicate that the quantities of induced dislocations reach a saturated value after 75 cycles in these alloys.

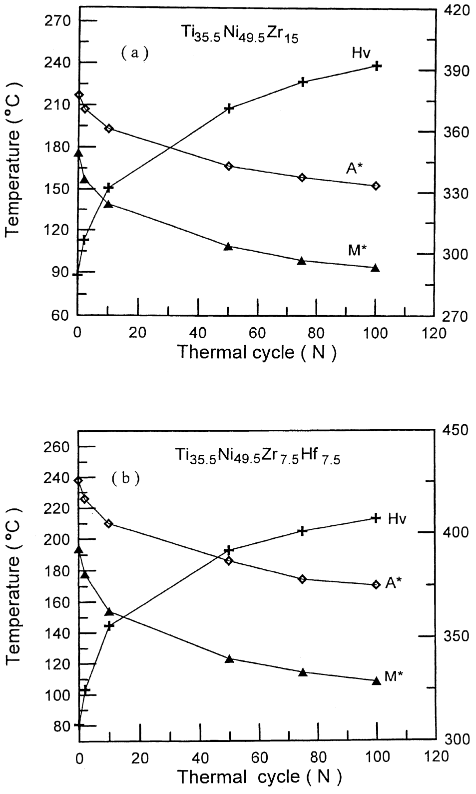

Fig. 9. Peak temperatures *A** and *M** and hardness Hv, vs. number of thermal cycles, *N*, for (a) $Ti_{35.5}Ni_{49.5}Zr_{15}$ alloy and (b) $Ti_{35.5}Ni_{49.5}Zr_{7.5}Hf_{7.5}$ alloy.

3.4. Strengthening effects of cold rolling and thermal cycling on martensitic transformation temperatures of $Ti_{35.5}Ni_{49.5}Zr_{7.5}Hf_{7.5}$ alloy

Fig. 10a and b shows the relationship between peak temperature *M** and hardness Hv for the cold-rolled and thermally-cycled $Ti_{35.5}Ni_{49.5}Zr_{7.5}Hf_{7.5}$ alloy. The results of cold-rolled and thermally-cycled $Ti_{35.5}Ni_{49.5}Zr_{15}$ alloy are also shown in Fig. 10. It was pointed out that any strengthening mechanism, which impedes the transformation shear can lower the transformation temperatures because the martensitic transformation involves a shear process [21,22]. This feature can be expressed as

$$Ms = T_o - K\Delta\sigma_y \qquad (1)$$

where the constant *K* contains the factors of proportionality between the critical shear stress and the yield stress $\Delta\sigma_y$, the equilibrium temperature T_o is a function of the chemical composition, and the yield stress $\Delta\sigma_y$ is regarded as proportional to the hardness.

In this study, both cold rolling and thermal cycling do not change the alloy's composition, hence T_o is a constant. In addition, both cold rolling and thermal cycling can strengthen the alloys by inducing dislocations, and therefore can raise the yield stress $\Delta\sigma_y$. As seen from Eq. (1), this feature should cause the *M** and *A** temperatures to be lowered by the strengthening effect. This prediction is qualitatively consistent with the results of Fig. 10. In Fig. 10, the slope represents the constant *K*, which is not the same for different strengthening processes. These *K* values indicate that cold rolling and thermal cycling can provide different strengthening mechanisms and exhibit different effects on transformation temperatures. As mentioned above, strengthening processes can introduce dislocations in these alloys. However, dislocations induced by cold rolling originate from the plastic deformation of martensite, and those induced by thermal cycling come from the thermal stress and transformation shear associated with B2↔B19′. A careful examination of Fig. 10 shows that the constant *K* of the $Ti_{35.5}Ni_{49.5}Zr_{7.5}Hf_{7.5}$ alloy is larger than that of the $Ti_{35.5}Ni_{49.5}Zr_{15}$ alloy for the same strengthening process. We propose that the *K* value is closely related to the inherent hardness of annealed TiNiZr or TiNiZr*X* alloys. The higher the annealed hardness, the larger the *K* value is. For example, the thermally-cycled $Ti_{35.5}Ni_{49.5}Zr_{7.5}Hf_{7.5}$ alloy has its annealed hardness at about 308 Hv and its *K*

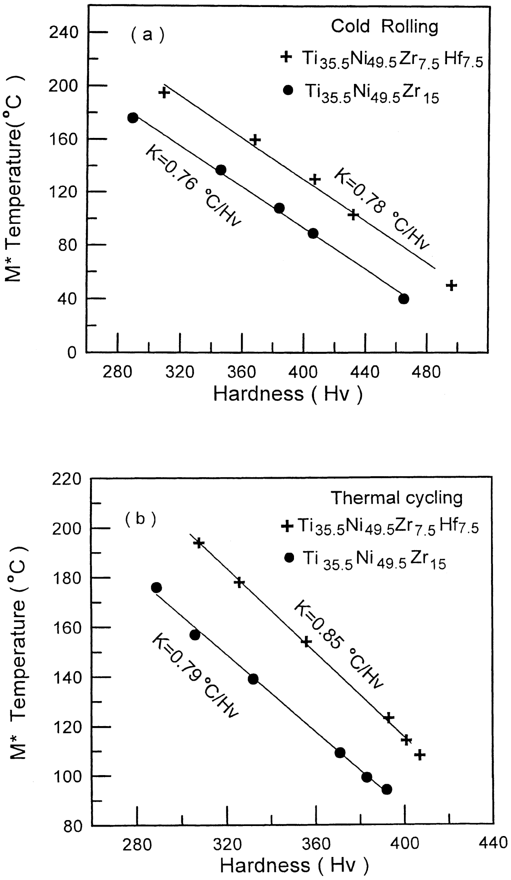

Fig. 10. The temperature *M** vs. hardness Hv for (a) cold-rolled and (b) thermally-cycled $Ti_{35.5}Ni_{49.5}Zr_{7.5}Hf_{7.5}$ and $Ti_{35.5}Ni_{49.5}Zr_{15}$ alloys.

value is found to be 0.85°C/Hv, which is larger than the thermally-cycled $Ti_{35.5}Ni_{49.5}Zr_{15}$ alloy (289 Hv, K = 0.79°C/Hv). This characteristic is also found in cold-rolled alloys, as shown in Fig. 10a. In other words, the depression of Ms(M*) and As(A*) temperatures by the strengthening mechanism is stronger for the alloys having a higher annealed hardness. As mentioned above, A alloys have a higher annealed hardness than B alloys. This feature can explain why the K value of $Ti_{35.5}Ni_{49.5}Zr_{7.5}Hf_{7.5}$ alloy is higher than that of $Ti_{35.5}Ni_{49.5}Zr_{15}$ alloy under the same strengthening process, as demonstrated in Fig. 10.

3.5. Aging effect on the $Ti_{30.5}Ni_{49.5}Zr_{10}Hf_{10}$ alloy

Fig. 11a and b shows the results of DSC measurements in 285°C aged $Ti_{30.5}Ni_{49.5}Zr_{10}Hf_{10}$ alloy and 200°C aged $Ti_{30.5}Ni_{49.5}Zr_{20}$ alloy, respectively. Both alloys are aged in the martensite phase. In Fig. 11, A_1* and A_2*, respectively indicate the first and second heating cycle for the specimen just after aging. From Fig. 11, the A_1* temperature is seen to increase with increasing aging time. This feature exhibits the phenomenon of martensite stabilization, the same behavior as reported in Cu-based SMAs [23–26]. Two mechanisms were proposed to explain the martensite stabilization in Cu-based SMAs: (i) reordering in the martensite, where the atomic rearrangement in martensite results in some change of the relative stability between parent and martensite [23,24]; and (ii) pinning or locking the interfaces of martensite/parent and martensite/martensite by aging-induced defects or precipitates [25,26]. Fig. 12a shows the TEM bright-field image of the martensite in a 285°C for 50 days aged $Ti_{30.5}Ni_{49.5}Zr_{10}Hf_{10}$ specimen. Fig. 12b–d shows the SADPs of Fig. 12a, in which the foil is parallel to $[100]_M$, $[010]_M$, and $[101]_M$ directions, respectively. No extra reflection spot can be observed in

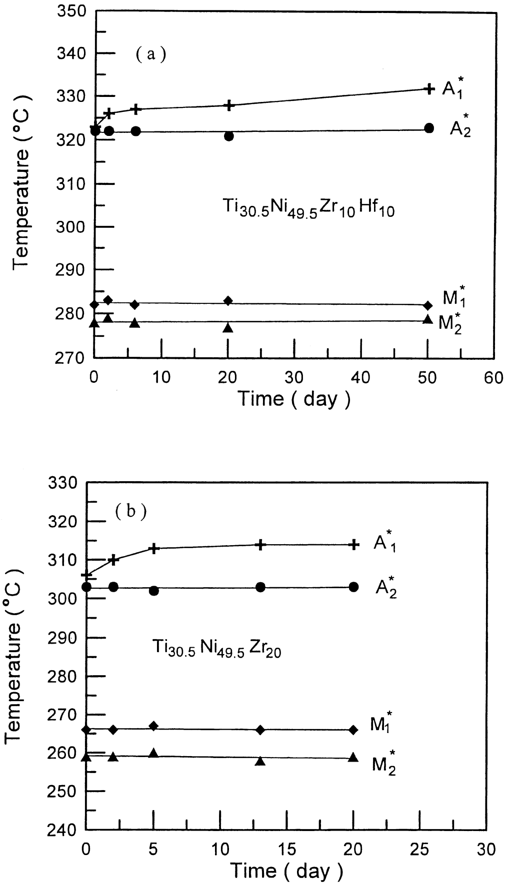

Fig. 11. Peak temperatures *A** and *M** and hardness vs. aging time for (a) $Ti_{30.5}Ni_{49.5}Zr_{10}Hf_{10}$ alloy and (b) $Ti_{35.5}Ni_{49.5}Zr_{15}$ alloy.

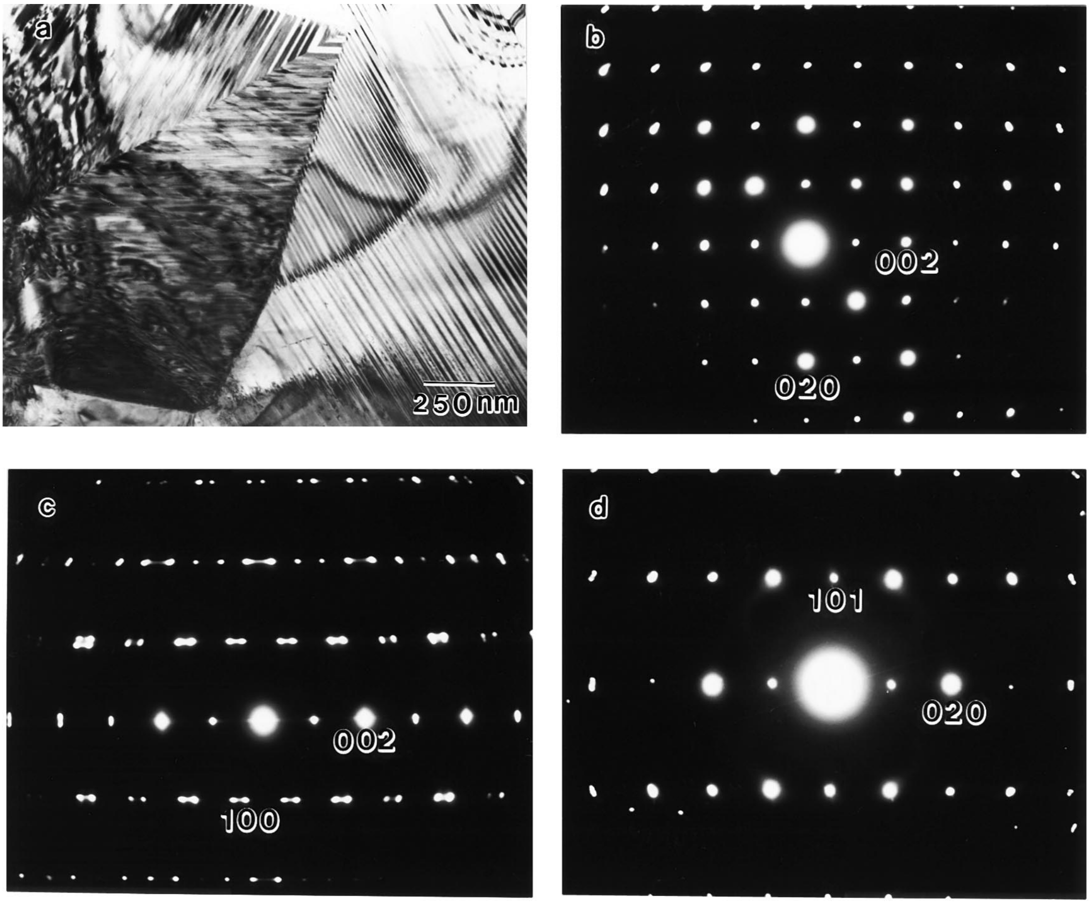

Fig. 12. (a) Bright-field image of martensite in 285°C × 50 days aged $Ti_{30.5}Ni_{49.5}Zr_{10}Hf_{10}$ alloy. (b)–(d) SADPs of (a) with (b) $[100]_M$ zone axis, (c) $[010]_M$ zone axis, and (d) $[101]_M$ zone axis.

Fig. 12. This feature implies that the mechanism of the reordering in martensite after the martensite stabilization may not occur. It has been reported that the interfaces between parent and martensite or martensite and martensite plates in the stabilized $Ti_{26.5}Ni_{48.5}Zr_{25}$ martensite may be pinned by point defects such as interstitial atoms (H, O, etc.) and quenched in vacancies [13]. We propose that the same phenomenon of martensite stabilization may also occur in the aged $Ti_{30.5}Ni_{49.5}Zr_{10}Hf_{10}$ alloy.

4. Conclusion

Martensitic transformation of $Ti_{50.5-X}Ni_{49.5}Zr_{X/2}Hf_{X/2}$ high temperature SMAs have been studied by DSC measurement, hardness test, and microstructural observation. The important conclusions are as follows.

(1) The annealed $Ti_{50.5-X}Ni_{49.5}Zr_{X/2}Hf_{X/2}$ alloys undergo a one-stage B2↔B19′ martensitic transformation in which the transformation peak temperature M^* increases from 50°C to 323°C with increasing X from 0 to 20 at.%. Under the same X, the transformation temperatures and hysteresis of $Ti_{50.5-X}Ni_{49.5}Zr_{X/2}Hf_{X/2}$ alloys are both larger than those of $Ti_{50.5-X}Ni_{49.5}Zr_X$ ones. The former alloys are harder than the latter due to the solid solution of Hf atoms in the matrix. Many second phase particles are found around the grain boundaries of the matrix and are identified as λ_1 phase for alloys with $X \geq 10$ at.%. Despite the existence of second phase particles, these alloys still exhibit good shape recovery that can reach about 80%.

(2) The martensite stabilization can be induced by cold-rolled $Ti_{35.5}Ni_{49.5}Zr_{7.5}Hf_{7.5}$ and $Ti_{35.5}Ni_{49.5}Zr_{15}$ alloys at room temperature. The hardness increment of the former alloy is larger than that of the latter under the same degree of cold rolling, owing to the former alloy having higher annealed hardness.

(3) A^* and M^* temperatures decrease and the hardness increases in the first 10 cycles of thermally-cycled $Ti_{35.5}Ni_{49.5}Zr_{7.5}Hf_{7.5}$ and $Ti_{35.5}Ni_{49.5}Zr_{15}$ alloys. The decrement of the A^* temperature of the

former alloy is larger than that of the latter at the same *N* due to the former alloy having the harder matrix.

(4) The strengthening effects of cold rolling and thermal cycling on Ms(*M**) temperatures of $Ti_{35.5}Ni_{49.5}Zr_{7.5}Hf_{7.5}$ and $Ti_{35.5}Ni_{49.5}Zr_{15}$ alloys are found to follow the equation $Ms = T_o - K\Delta\sigma_y$. Strengthening processes of cold rolling and thermal cycling have their different *K* values. The annealed hardness of $Ti_{35.5}Ni_{49.5}Zr_{7.5}Hf_{7.5}$ alloy is higher than that of $Ti_{35.5}Ni_{49.5}Zr_{15}$ alloy. This feature causes the former alloy to have a higher *K* value than the latter under the same strengthening process.

(5) In the $Ti_{30.5}Ni_{49.5}Zr_{10}Hf_{10}$ alloy, a thermally-induced martensite stabilization occurs after aging in the martensite phase. This characteristic may be caused from the pinning/locking effect, i.e., the interfaces of martensite/parent or martensite/martensite are pinned by aging-induced point defects.

Acknowledgments

The authors sincerely acknowledge the financial support of this study by the National Science Council (NSC), Republic of China, under the Grant NSC 86-2216-E002-033.

References

[1] Miyazaki S, Kotsuka K, Suzuki Y. Transformation pseudoelasticity and deformation behavior in a Ti–50.6% Ni alloy. Scr Metall 1981;15:281–87.

[2] Miyazaki S, Imai T, Igo Y, Kotsuka K. Effect of cyclic deformation on the pseudoelasticity characteristics of Ti–Ni alloys. Metall Trans 1986;17A:115–20.

[3] Eckelmeyer KH. The effect of alloying on the shape memory phenomenon in nitinol. Scr Metall 1976;10: 667–72.

[4] Hwang CM, Wayman CM. Phase transformation in Ti–Ni–Fe, Ti–Ni–Al and TiNi alloys. Scr Metall 1983;17:1345–50.

[5] Hwang CM, Meichle M, Salamon MB, Wayman CM. Transformation behavior of a $Ti_{50}Ni_{47}Fe_3$ alloy: III. Martensitic transformation. Philos Mag 1983;47A: 177–91.

[6] Lindqist PG, Wayman CM. Shape memory and transformation behavior of martensitic Ti–Pd–Ni and Ti–Pt–Ni alloys. In: Duering TW, Melton KN, Stockel D, Wayman CM, editors. Engineering Aspects of Shape Memory Alloys. London: Butterworth, 1990. p. 58.

[7] Lo YC, Wu SK, Wayman CM. Transformation heat as a function of ternary Pd additions in $Ti_{50}Ni_{50-X}Pd_X$ alloys with $X = 20-50$ at.%. Scr Metall 1990;24: 1571–6.

[8] Wu SK, Wayman CM. Martensitic transformation and the shape memory effect in $Ti_{50}Ni_{10}Au_{40}$ and $Ti_{50}Au_{50}$ alloys. Metall 1987;20:359–76.

[9] Hsieh SF, Wu SK. Room-temperature phase observed in $Ti_{53-X}Ni_{47}Zr_X$ high-temperature shape memory alloys. J Alloys Compd 1998;266:276–82.

[10] Meisner L, Sivokha V. Deformation of crystal lattice in the process of martensitic transformation in alloys of $Ni_{50}Ti_{50-X}Zr_X$. J Phys IV 1995;C8:765–9.

[11] Hsieh SF, Wu SK. A study on lattice parameters of martensite in $Ti_{50.5-X}Ni_{49.5}Zr_X$ shape memory alloys. J Alloys Compd 1998;270:237–41.

[12] Mulder JH, Mass JH, Beyer J. Martensitic transformations and shape memory effects in Ti–Ni–Zr alloys. Proc. Int. Conf. on Martensitic Transformations, Monterey, California (July 20–24, 1992).

[13] Hsieh SF, Wu SK. A study on Ti-rich TiNiZr shape memory alloys. Mater Charact 1998;41:151–62.

[14] Lin HC, Wu SK. Strengthening effect on shape recovery characteristic of the equiatomic TiNi alloy. Scr Metall 1992;26:59–61.

[15] Han XD, Zou WH, Wang R, Zhang Z, Yang DZ, Wu KH. The martensite structure and aging precipitates of a TiNiHf high temperature shape memory alloys. J Phys IV 1995;C8:753–8.

[16] Humbeck JV, Stalmans R, Chanadrasekaran M, Delay L. On the stability of shape memory alloys. In: Duering TW, Melton KN, Stockel D, Wayman CM, editors. Engineering Aspects of Shape Memory Alloys. London: Butterworth, 1990. p. 96.

[17] Suzuki Y, Horikawa H. Thermal hysteresis in Ni–Ti and Ni–Ti–*X* alloys and their applications. In: Liu CT, Kunsimann H, Otsuka K, Wuttig M, editors. Shape-Memory Materials and Phenomena-Fundamental Aspects and Applications. Pittsburgh, PA: Materials Research Society, 1992. p. 389.

[18] Lin HC, Wu SK, Chou TS, Kao HP. The effects of cold rolling on the martensitic transformation of an equiatomic TiNi alloy. Acta Metall 1991;39:2069–80.

[19] Lin HC, Wu SK, Lin JC. The martensitic transformation in Ti-rich TiNi shape memory alloys. Mater Chem Phys 1994;37:184–90.

[20] Miyazaki S, Igo Y, Otsuka K. Effect of thermal cycling on the transformation temperatures of TiNi alloys. Acta Metall 1986;34:2045–51.

[21] Cohen M, Machlin ES, Paranjpe VG. Thermodynamics in Physical Metallurgy. Metals Park, OH: ASM, 1950. p. 242.

[22] Hornbogen E. The effect of variables on martensitic transformation temperatures. Acta Metall 1991;33: 595–601.

[23] Scarsbrook G, Stobbs WM. The martensitic transformation behavior and stabilization of rapidly quenched Cu–Zn–Al ribbons. Acta Metall 1987;35:47–56.

[24] Arab AA, Chanadrasekaran M, Alers M. Martensite aging and its stabilization in Cu–Zn–Al shape memory alloys. Scr Metall 1984;18:709–14.

[25] Ahlers M. The stabilization of martensite in Cu–Zn–Al. Proc. Int. Conf. on Martensitic Transformation, Nara, Japan (August 26–30, 1986).

[26] Wu MH, Wayman CM. Isothermal aging of martensite in a Cu–Zn–Al shape memory alloy. Mater Sci Forum 1990;56–58:553–8.